Remote Gas Detection Using Millimeter-Wave Spectroscopy for Counter Bio-Terrorism

Matthew Szlazak[a], Seng Yiep Yam[a], Dejan Majstorovic[b], Hedley Hansen[b], Derek Abbott[a]
[a]Centre for Biomedical Engineering (CBME) and Department of Electrical & Electronic Engineering, The University of Adelaide, SA 5005, Australia
[b]EWD, DSTO, P.O. Box 1500, Edinburgh, SA 5111, Australia

ABSTRACT

The mm-wave (10-110 GHz) frequency band contains the fundamental rotational resonance frequencies of many molecular gases composed of carbon, nitrogen, oxygen and sulfur. The high specificity of the rotational spectra to organic molecules affords mm-wave spectroscopy having potential use in remotely sensing atmospheric pollutants and the detection of airborne chemicals is gaining importance for arms control treaty verification, intelligence collection and environmental monitoring. This paper considers RF receiver systems for remote chemical detection measurements based on mm-wave spectral line emissions. It discusses the design, performance and operation of specific receiving systems for detecting the presence of ammonia in laboratory based transmit-and-receive experiments.

Keywords: remote sensing; remote gas detection; millimeter wave spectroscopy; low-noise front-end receivers; spectrum analyzer; K-band; W-band.

1. INTRODUCTION

The millimeter wave region of the electromagnetic spectrum, occupying the frequency range from 30 GHz to 300 GHz (1 mm to 99 mm wavelength), lies between microwave and submillimeter (T-ray) bands. Figure 1 depicts the location of the region on the electromagnetic spectrum.[1]

Millimeter wave spectroscopy utilizes the unique specific absorption and emission spectral lines of chemical structures in order to identify materials[2]. The lines are specific to particular molecular configurations because they are associated with the existence of associated electric dipole structures. At micro and millimeter wave frequencies exist the fundamental rotational frequencies for diatomic molecules composed of carbon, nitrogen and sulfur, thus mm-wave spectral line measurements are invaluable for atmospheric ozone studies and for understanding the chemistry existing in outer space.

In contrast with outer space and upper atmospheric regions, the exploitation of mm-wave spectroscopy in the terrestrial environment has proved unattractive. This relates partly to the natural radiation spectrum of most gaseous materials being dominated by transitions between vibrational states that give rise to emissions in the higher IR region of the electromagnetic spectrum. Those lower energy rotational states, that tend to give rise to mm and microwave RF emissions, typically have low radiation levels at everyday temperatures and are broadened due to the collision-dominated molecular interactions that occur at atmospheric temperatures and pressures.

New emerging micro-technologies are playing a role in allowing the measurement of low signal RF radiation processes to be possible in the lower atmosphere. The emergence of high RF sensors, that utilize GaAs and InP based technologies, is poised to provide the 10's-of Giga-byte-samples/sec rate and broadband signal handling capability for real-time remote sensing applications at mm-wave and submillimeter frequencies. Modern radiometers are capable of detecting 0.01K signals[3] and as these levels improve, spectral methods will be increasingly exploited for atmospheric constituent studies. In particular, remote sensing using millimeter waves is of interest due to the strong interaction of these waves with airborne molecules associated with chemical and nuclear proliferation facilities[4], and because compared to optical and IR waves, mm-waves suffer far less attenuation in the atmosphere in the presence of water vapor, smoke, fog and dust[2].

Further Author information: (Send correspondence to D. Abbott)
D. Abbott: E-mail: dabbott@eleceng.adelaide.edu.au
H. Hansen: Email: hedley.Hansen@dsto.defence.gov.au

Biomedical Applications of Micro- and Nanoengineering, Dan V. Nicolau, Abraham P. Lee, Editors,
Proceedings of SPIE Vol. 4937 (2002) © 2002 SPIE · 0277-786X/02/$15.00

This paper describes initial studies towards the development of remote chemical detection systems for defence related surveillance applications. The absorption effects associated with the presence of ammonia gas in air have been measured with altered broadband Electronic Support Measure (ESM) receiver architectures that operate at Ka-band (26-40 GHz) frequencies.

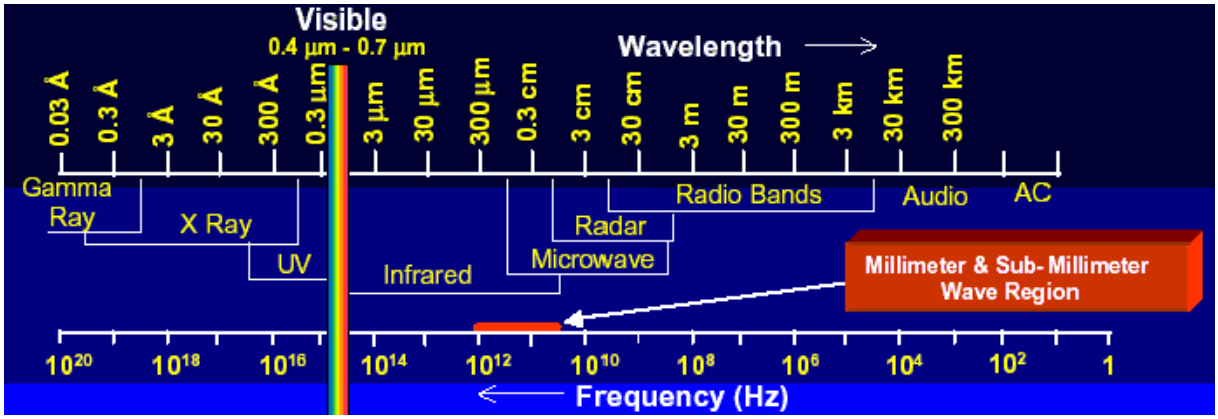

Figure 1: Electromagnetic Spectrum [1]

1.1 SPECTROSCOPIC PRINCIPLES

Molecular rotation spectroscopy is based on the permanent intrinsic dipole moment of a molecule interacting with an oscillatory electric field component of radiation causing a transition between the molecules rotational states.

The rotational energy states available to a molecule are governed by angular momentum J. Classically, angular momentum is defined as

$$J = J_A^2 + J_B^2 + J_C^2 \tag{1}$$

where A, B and C are the three dimensional axes and J_i is the component angular momentum associated with the i_{th} axis. A molecule's rotational energy is expressed as

$$E = \frac{J_A^2}{2I_A} + \frac{J_B^2}{2I_B} + \frac{J_C^2}{2I_C} \tag{2}$$

where I_i is the component moment of inertia about the i_{th} axis.

Asymmetric molecular configurations are typically described in terms of two symmetric cases, prolate tops in which axis $B = C$ and oblate tops in which $A = B$. Most molecules fall into the category of either near prolate tops with $I_A < I_B \sim I_C$ or near oblate tops with $I_A \sim I_B < I_C$. This paper describes spectral line effects associated with ammonia (NH_3), a near prolate top molecule[5]. For near prolate top molecules, Equation (2) can be expressed as

$$E = \frac{1}{2}\left(\frac{J^2}{I_B} - \frac{J_A^2}{I_B} + \frac{J_A^2}{I_A}\right). \tag{3}$$

Because J^2 is quantized in units of $J(J+1)\hbar^2$ and J in units of $K^2\hbar^2$ (where quantum number K is allowed unit values ranging from $-J$ to J) Equation (3) is rewritten as

$$E = \frac{1}{2}\frac{\hbar^2 J(J+1)}{I_B} + \frac{\hbar^2 K^2}{2}\left(\frac{1}{I_A} + \frac{1}{I_B}\right) \tag{4}$$

which describes the energy states available to ammonia-type molecules.

The measurements to be reported here are associated with inversion of the ammonia molecule. For ammonia the two mirror image configurations shown in Figure 2 exist.[5] A potential energy barrier between these configurations accommodates a resonant interaction that causes the rotational lines to split and transitions occur between the components of these levels. Figure 10 shows[5] the rotational levels for $J < 9$ for which rotationally split energy levels are represented by the simple equation

$$\upsilon = \upsilon_0 - aJ(J+1) - (a-b)K^2 \tag{5}$$

where $\nu_o = 23.787$, $a = 0.151$ and $(a-b) = -0.211$ GHz.

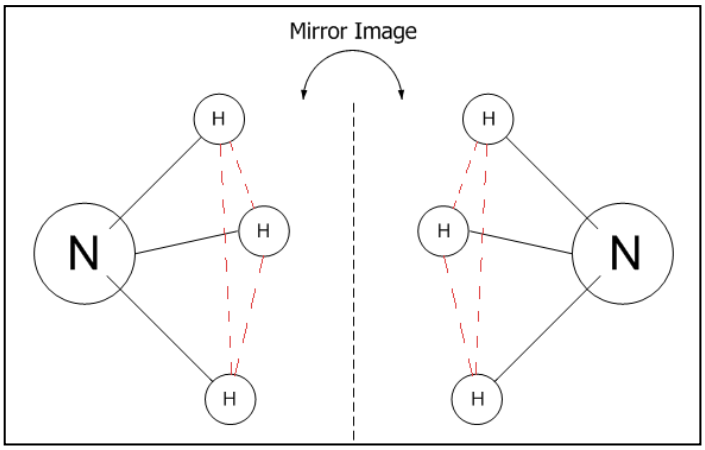

Figure 2: Ammonia Chemical Structure Mirror Image

1.2 EINSTEIN COEFFICIENTS AND ABSORPTION AND EMISSION

Einstein showed between any two energy levels either (i) spontaneous emission with probability A_{ul} (u depicts the upper energy level; l indicates the lower energy state), (ii) absorption with probability $B_{lu}U$ (where U is the average density of the radiation field), or (iii) simulated emission with probability $B_{ul}U$ is possible. The coefficients A_{ul}, B_{lu} and B_{ul} are dependent according to

$B_{lu} = (g_2 / g_1)B_{ul}$ (where g_i is the degeneracy of the ith state) and

$A_{ul} = 8\pi h\nu^3 / c^3 B_{ul}$ (where h is Plank's constant, ν is the frequency and c is the speed of light).

These dependencies are linked to the radiation field following Planck's distribution, and to the molecules exhibiting occupancy of the available states in accordance with Boltzmann distribution.

It is significant that the Einstein coefficients associated with any material are related[5] to macroscopic opacity and emission coefficients κ and ε. The absorption of radiation as it passes through a material is described by Beer-Lambert Law, viz.,

$$\frac{dI}{ds} = -\kappa_\nu I_\nu + \varepsilon_\upsilon \tag{6}$$

where *ds* is the slab of thickness *dI* is the change in intensity, κ is the opacity and ε is the emissivity. The Einstein coefficients have been used to demonstrate[5] that this equation of transfer becomes

$$\frac{dI}{ds} = -\frac{h\nu}{c}\left(N_l B_{lu} - N_u B_{ul}\right) I_\nu \varphi(\nu) + \frac{h\nu}{4\pi} N_u A_{ul} \varphi(\nu) \tag{7}$$

where N_i denotes the occupancy of the *i*th state, *I* the intensity and *Φ(v)* the line profile.
From inspection of Equation's (7) and (8) the opacity κ_v is given by

$$\kappa_\upsilon = -\frac{h\nu}{c}\left(N_l B_{lu} - N_u B_{ul}\right) \tag{8}$$

that has been re-written as

$$\kappa_\nu = \frac{c^2}{8\pi} \frac{1}{\upsilon} \frac{g_2}{g_1} A_{ul} \left[1 - \exp(-\frac{h\upsilon}{kT})\right] \varphi(\nu) \tag{9}$$

where *k* is Boltzmann's constant and *T* is the temperature. Significantly, this links the macroscopic absorption coefficient with the radiation rate associated with a particular spectral line profile. From the literature[5] Einstein coefficient A_{ij} for appropriate NH_3 energy states, can be used to calculate the opacity of the gas in order to compare it with the value determined from absorption measurements.

2. METHODOLOGY

2.1 PASSIVE DETECTION

Passive RF sensing involves the detection of naturally occurring electromagnetic radiation with radiometers. Passive techniques are widely used in radio astronomy and atmospheric observations, made with antennas pointing away from the surface of the earth, located either on land or on an aircraft.

In order to understand how the capability of a receiver for spectral line remote sensing is related to its performance figures, the detection scenario depicted in Figure 3 (which pertains to a passive detection of a pollutant cloud) is considered. This closely parallels previous approaches.[3] Figure 3 considers a cloud of gas pollutant of brightness B_c and thickness *D* imbedded in background of brightness B_g. In addition, a radiometer from an aerial platform looking at the cloud will also be sensitive to a contribution from the atmosphere B_a itself. The total brightness associated with the radiation detected can be expressed as

$$B_T = B_c e^{-\tau_c} + (B_g - B_c) e^{-(\tau_a + \tau_c)} + B_a \tag{10}$$

where τ_c is the optical thickness of the cloud, and τ_a is the optical thickness of the atmosphere between the sensor and the cloud. The optical thickness τ is defined to be $\tau = \kappa D$ where κ is the opacity as before.

At radio frequencies, Planck's Law allows brightness to be considered as

$$B = \frac{2kT}{\lambda^2} \tag{11}$$

where λ is the wavelength and so Equation (10) becomes

$$T_T = T_c e^{-\tau_c} + \left(\varepsilon_g T_g - T_c\right) e^{-(\tau_a + \tau_c)} + T_a \tag{12}$$

where for backgrounds of emissivity ε_g, $B_g = \varepsilon_g T_g$. Typically τ_a is a minor term, therefore Equation 12 approximates to

$$T_T = T_c(1-e^{-\tau_c}) + \varepsilon_g T_g e^{-\tau_c} + T_a \tag{13}$$

Were the pollutant cloud not present, $T_T = \varepsilon_g T_g + T_a$. Consequently, the observable signal[3] associated difference between these T_T values is

$$\Delta T_{obs} = (T_c - \varepsilon_g T_g)(1-e^{-\tau_c}) \approx (T_c - \varepsilon_g T_g)\tau_c \,. \tag{14}$$

The detection system must be sensitive to T_{obs} signal levels. However because the sensitivity of a radiometric receiver is given by

$$\Delta T_s = \frac{T_{system}}{\sqrt{B\tau}}, \tag{15}$$

the observed signal-to-noise ratio is

$$SNR = \frac{\Delta T_{obs}}{\Delta T_s}. \tag{16}$$

Equations 14 and 16 relate the detectability of spectral absorption lines (in terms of the optical thickness parameter) to the noise performance of a receiver. The environmental background $(T_c - \varepsilon_g T_g)$ of any standoff measurement affects the observable signal level. Figure 4 depicts curves of observed signal levels associated with receivers of different sensitivities (0.01, 3, 9, and 15 dB) as a function of optical depth for a particular air-to-ground scene (T_g=300, T_c=80, ε_g=0.5).

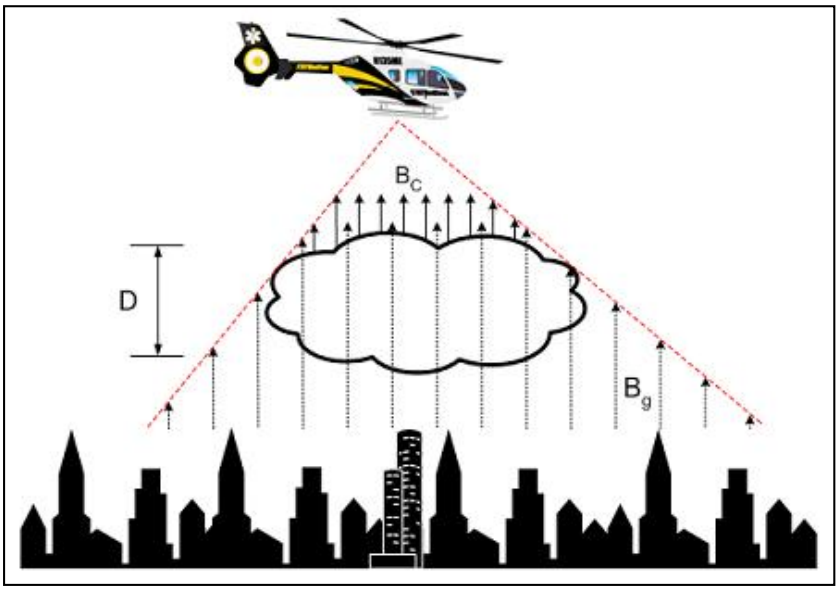

Figure 3: Passive Detection Scenario

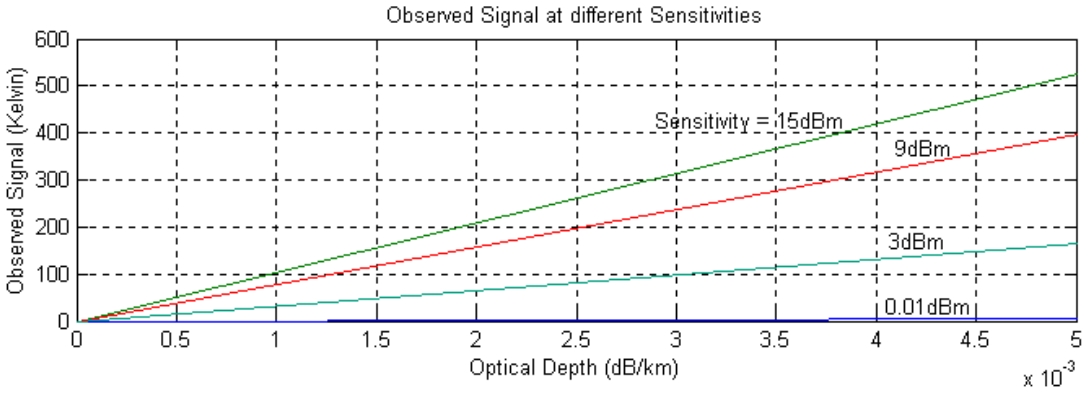

Figure 4: Observed Signal at different Sensitivities

2.2 ACTIVE DETECTION

Active remote sensors process transmitted electromagnetic radiation with tuned receiver systems. Figure 5 depicts a bistatic arrangement where the receiver and transmitter are displaced from each other. The received signal is given by the radar equation

$$P_R = \frac{P_T G_T A_R}{4\pi R^2} \tag{17}$$

where the terms have their usual meaning. For radar emissions propagating through an absorbing medium of optical thickness τ, the attenuated signal received becomes

$$P_R = P_R e^{-\tau} \tag{18}$$

The system would measure a signal change given by

$$S_{obs} = P_R (1 - e^{-\tau}) \tag{19}$$

with an associated signal-to-noise ratio of $S/N = S_{obs} / \Delta T_s$ where T_s is given by Equation (15). Active sensing is more sensitive than passive detection because coherent sources operate at signal levels far above background levels. Active measurements are only to be reported due to the limitations associated with the SNR performance of the receivers that were used for measurements.

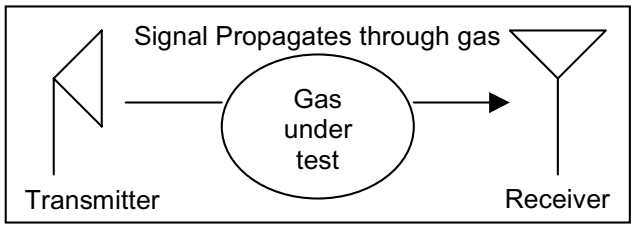

Figure 5: Active Remote Sensing Scenario Diagram

3. RF SPECTROSCOPIC RECEIVER DEVELOPMENT

Two RF Receiver architectures have been considered, a block down converter with an input range of 24 to 37 GHz and a direct receiver with an input range of 26.5 to 40 GHz. Both architectures have attractive features. Down-converters allow a RF sensing capability to be readily accommodated as an add-on front-end to already existing lower frequency microwave receiving systems. Direct receivers involve simple crystal video approach architectures that avoid mixing down for amplification stages at lower IFs. This approach is being increasingly deployed in operational miniaturised MMIC-based RF front-ends mm-wave imaging cameras[7].

3.1.a RECEIVER ARCHITECTURES - BLOCK DOWN-CONVERTER

The down-converter used is based on heterodyning and its component stages are as shown in Figure 6. The signal flow of the system is such that the signal is received through the antenna and passes through a WR28 waveguide, where it is then mixed with the local oscillator and down-converted to a frequency in the range 1 to 20 GHz. The receiver is a block down-converter as the whole input frequency bandwidth is down converted by 38 GHz to an intermediate frequency [$f_{IF} = | f_R - (f_{LO})|$], maintaining the same block bandwidth[8]. The local oscillator is a 19 GHz PLL (phase locked loop) oscillator; the 19 GHz signal is multiplied by two and mixed with the received signal. The down-converted signal passes from the receiver via a coaxial cable connection to a measuring device such as a spectrum analyser.

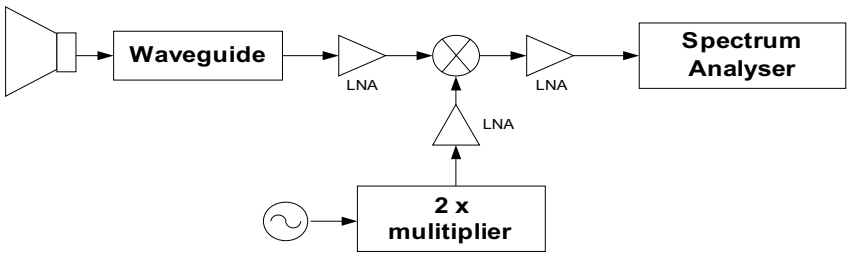

Figure 6: Down-Converter Structure

3.1.b Receiver Architectures - Direct Receiver

The block diagram of the direct receiver is shown in Figure 7. The stages outlined consist of an antenna, which receives the signal in the range 26.5 to 40 GHz, the Dicke switch, which provides a reference load to stabilise the system,[5] the isolator, which blocks the unwanted signal reflections and the cascaded RF amplifiers, which prepare the signal for detection. The amplifiers provide a gain of approximately 50 dB.

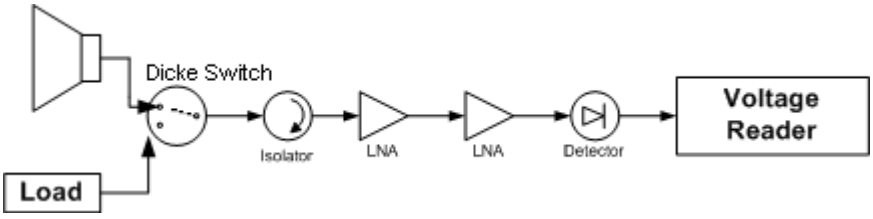

Figure 7: Direct Receiver Structure

The performance of these systems are characterised by measuring the gain and noise and using these values to determine the receiver sensitivity. Gains were determined by measuring the output power for a given input power and the sensitivities were obtained by doing a Y-factor noise figure measurement.

These specifications are summarised in Table 1. The down converter characterisation results showed that the performance of the receiver from 24 to 34 GHz is relatively constant with a gain of approximately 40 dB and a sensitivity of –50 dBm. The direct receiver results showed that the performance of the receiver is constant throughout the bandwidth. The gain of the system is approximately 45 dB and the sensitivity is close to –54.56 dBm on average.

Regarding the spectroscopic measurements to be described, the similarity in performance suggests it is necessary only to report on the measurements associated with one of these systems.

Table 1: Spectroscopic Receiver Specifications

Down Converter		**Direct Receiver**	
RF Input Range	24 to 37 GHz	RF Input Range	26.5 to 40 GHz
LO Frequency	38 GHz (2 x 19 GHz)	Noise Figure	9.54 dB (mean)
IF Frequency Range	1 to 20 GHz	Sensitivity	-54.56 dBm (mean)
Noise Figure	15.48 dB (mean)	Radiometric Sensitivity	$\Delta T < 2.63$ K
Sensitivity	-50.39 dBm (mean)	Gain	44.89 dB (mean)
Radiometric Sensitivity	$\Delta T < 2.75$ K		
Gain	39.34 dB (mean)		

4. KA BAND SPECTRA FOR AMMONIA

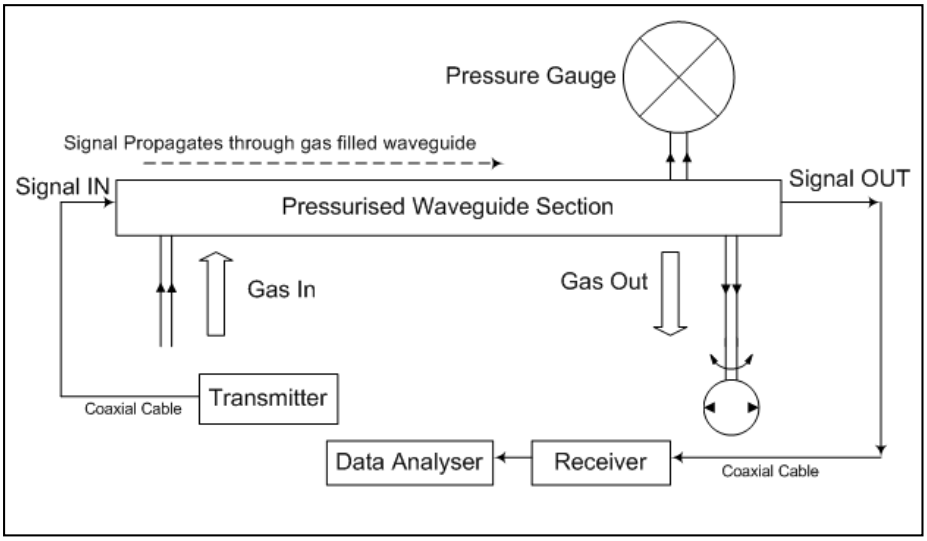

Figure 8: Gas Detection Experiment Layout

The experimental setup used for the spectroscopy measurements is shown in Figure 8. It consists of a pressurised waveguide (WR-28) in which millimetre wave signals propagate from transmitter to receiver. The waveguide comprises a gas inlet, a pressure gauge, and a gas outlet to which a pump is connected. The pump draws the gas through the waveguide until a pressure of 200 millibars is achieved after which the inlets are then sealed to hold the gas inside.

Using this set-up with a network analyser as the source, frequency ramped mm-wave signals (input power of 5 dBm over the frequency range 23–40 GHz) were launched into the waveguide. The network analyser has a very stable response, very high gain (70dB), very high sensitivity (-100 dBm) and a dynamic range of 80 dB.

Figure 9 shows the received power measured for both ammonia and pure air in the waveguide, using the network analyser's built in tracking receiver probe instead of the receiver system. Ammonia's presence in the waveguide causes lower transmitted signal levels at 23-28 GHz compared to air-only filled waveguide measurements. The asterisks on the ammonia plot represent the known frequencies corresponding to J-K transitions (Figure 10, Table 2) associated with the NH_3 inversion. The 200mBar pressure in the waveguide broadens the attenuation peaks into a continuum.

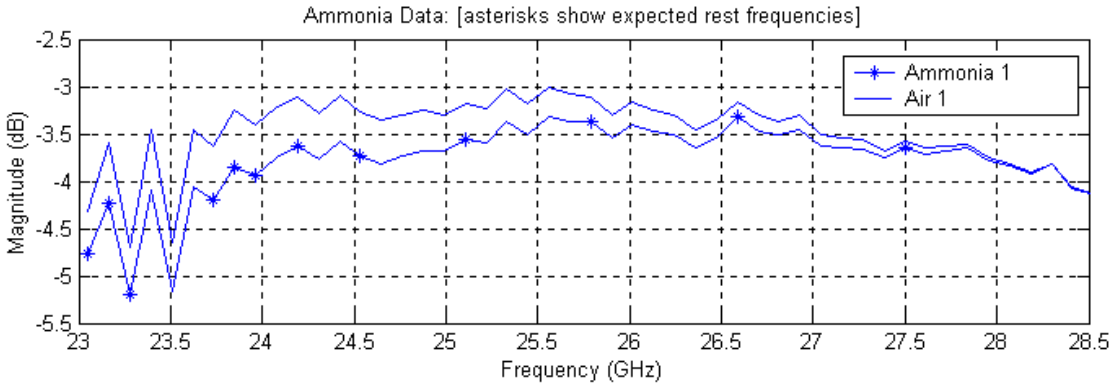

Figure 9: Network Analyser Ammonia Data

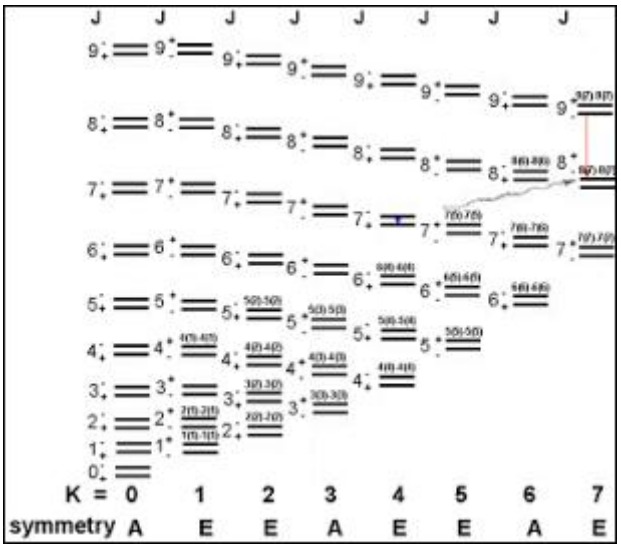

Figure 10: NH_3 J-K Transition Energy Level Diagram [5]

Table 2: NH_3 *J-K* Transition Frequencies [9]

Frequency (GHz)	Quantum Number	Frequency (GHz)	Quantum Number
	J(K) –J(K)		***J(K) –J(K)***
23.098	2(1) – 2(1)	24.532	5(5) – 5(5)
23.232	8(7) – 8(7)	25.056	6(6) – 6(6)
23.692	1(1) – 1(1)	25.715	7(7) – 7(7)
23.868	3(3) – 3(3)	26.518	8(8) – 8(8)
24.139	4(4) – 4(4)	27.477	9(9) – 9(9)
24.205	10(9) – 10(9)		

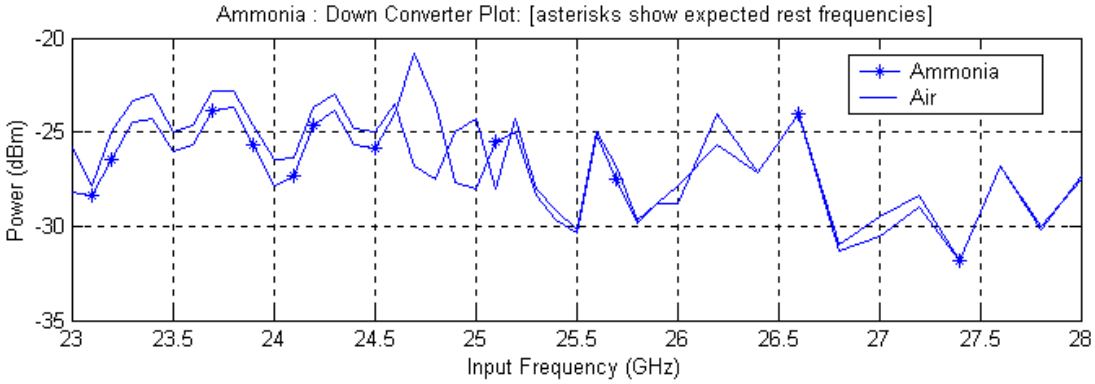

Figure 11: Down-Converter Spectroscopy Results

The network analyser results were then replicated using the down-converter system to receive the transmissions instead of the network analyser's probe. The measurements shown in Figure 11 indicate that for 23-28 GHz signals the same effect as that depicted in Figure 9 is shown.

5. DISCUSSION AND CONCLUSION

This paper has described a preliminary study involving a bistatic transmitter receiver arrangement where mm-wave sensing is used to discern ammonia concentrations in a waveguide. Absorption coefficient values for ammonia, obtained from the WEBGEN[6] and HITRAN 1996 database are typically ~5×10^{-21} $cm^2molecule^{-1}$ across the band of interest. Assuming ideal gas laws, we estimate that the concentration of ammonia in the waveguide relates to particle density of 2.5×10^{21} cm^{-3} and therefore an absorption coefficient of 0.87 dB/cm. This is consistent with the attenuation exhibited by the network analyzer measurements.

These receivers as they stand, are inadequate for passive standoff measurements of trace gas concentrations in the atmosphere. Figure 4 showed the minimum observed temperature associated with optical depth for a range of measuring system sensitivities. The 15 dB noise curve exhibits 10^3 K measurements whereas 0.01 K are needed for the trace element studies[5]. Such low noise figures are typically found in cryogenically cooled InP front-end receivers associated with high altitude and astronomical telescope observations[10].

Despite the low sensitivity limitations of these measurement systems, we have discerned spectral line features associated with the inversion of ammonia and this has been achieved with measurements where the discrete spectral line features are not resolvable[11]. Clearly, broadened spectral features might be adequate for identifying large organic configurations such a mustard gas, sarin and soman[2]. This supports the view that the performance requirements for anti-terrorism surveillance systems might be less stringent than that considered necessary for conventional astronomical spectroscopy systems[12].

Future work will concentrate on developing receiver front-ends sensitive enough for passive measurement and to identify the spectral features of atmospheric pollutants associated with rocket and other exhaust fuels. In addition, studies should be extended to higher frequencies in the sub-millimetre-wave region of the electromagnetic spectrum. At room temperatures, the natural frequencies of most molecules lie in the infrared, and confining receiver development to below 100 GHz is restrictive. Ozone mid-latitude observations and a plethora of other atmospheric constituent gas studies (eg, NO_2, CO, CH_3CL etc) are based on spectral line measurements above 100 GHz, and a recent report[13] suggests that 600 GHz might be useful for covert anthrax detection in civilian security applications.

REFERENCES

1. R.G. Reeves, A. Anson, D. Landen (eds), *Manual Of Remote Sensing,* **Vol. 1**, First Edition*,* Falls Church, 1975
2. A.C. Samuels, J.O. Jensen, R.D. Suenram, A.H. Walker, D. Woolard, "Microwave Spectroscopy of Chemical Warfare Agents: Prospects for Remote Sensing*," Proc. SPIE Passive Millimeter-Wave Imaging Technology III*, 7 April 1999 Orlando, FL, USA, **Vol. 3703**, pp. 121-129, 1999
3. N. Gopalsami and A.C. Raptis, "Millimetre Wave Sensing of Airborne Chemicals*," IEEE Transactions on Microwave Theory and Techniques*, **Vol.49**, No. 4, pt. 1, pp. 646-653, 2001
4. N. Gopalsami, A.C. Raptis, "Millimetre-wave Imaging of Thermal and Chemical Signatures," *Proc. SPIE Passive Millimeter-Wave Imaging Technology III*, 7 April 1999 Orlando, FL, USA, **Vol. 3703**, pp. 130-138, 1999
5. K. Rohlfs, T.L. Wilson, *Tools of Radio Astronomy,* Springer Verlag, New York, 1999
6. B. Quine, *WEBGEN: Spectroscopic Absorption Calculator* (Online computations for laboratory gas cells), University of Toronto, 2001. (http://nitrogen3.atmosp.physics.utoronto.ca/webgen_lab_in.html)
7. D. G. Gleed, A. H. Lettington, R. Appleby, S. Price, N. A. Salmon, R. N. Anderton, G. N. Sinclair, J. R. Borrill, "Operational issues for passive millimetre wave imaging system," Proc. SPIE Passive Millimeter-Wave Imaging Technology, 21-22 April 1997 Orlando, FL, USA, **Vol. 3064**, 1997
8. G.L. Hey-Shipton and A.W. Denning, *Millimetre Wave Block Converters,* **Vol 16**, No. 6 Nov/Dec 1989*,* Watkins-Johnson Company, 1989
9. F. Lovas, *National Institute of Standards and Technologies,* 1992
10. M.G. Case, C. Pobanz, S. Weinreb, M. Matloubian, M. Hu, M. Wetzel, P. Janke and C. Ngo, *"Low-Cost, High-Performance W-Band LNA MMICs for Millimeter-Wave Imaging," Proc. SPIE Passive Millimeter-Wave Imaging Technology IV*, Apr 26-Apr 26 2000, Orlando, FL, USA, **Vol. 4032,** pp.89-96, 2000
11. N.A. Salmon, R. Appleby, "Carbon monoxide detection using passive and active millimetre wave radiometry*," Proc. SPIE Passive Millimeter-Wave Imaging Technology IV*, Apr 26-Apr 26 2000, Orlando, FL, USA, **Vol. 4032**, pp. 119-122, 2000
12. C. Martin, J. Lovberg, S. Clark, J. Galliano, "Real time passive millimetre-wave imaging from a helicopter platform," *Proc. SPIE Passive Millimeter-Wave Imaging Technology IV*, Apr 26-Apr 26 2000, Orlando, FL, USA, **Vol. 4032**, pp. 22-28, 2000
13. E.R. Brown, D. L. Woolard, A.C. Samuels, T. Globus and B. Gelmont, "Remote Detection of Bioparticles in the THz Region," *Proc. 2002 IEEE MTT-S International Microwave Symposium*, **Vol. 3**, pp.1591-1594, 2002